Published in final edited form as:

Cancer Immunol Res. 2021 May ; 9(5): 568–582. doi:10.1158/2326-6066.CIR-20-0342.

Neutral Sphingomyelinase 2 Heightens Anti-Melanoma Immune Responses and Anti–PD-1 Therapy Efficacy

Anne Montfort[1,2], **Florie Bertrand**[1,2], **Julia Rochotte**[1,2,3], **Julia Gilhodes**[4], **Thomas Filleron**[4], **Jean Milhès**[1,2], **Carine Dufau**[1,2,3], **Caroline Imbert**[1,2], **Joëlle Riond**[1,2], **Marie Tosolini**[1], **Christopher J. Clarke**[5], **Florent Dufour**[6,7], **Andrei A. Constantinescu**[6,7], **Nilton De França Junior**[6,7], **Virginie Garcia**[1,2], **Michel Record**[1,8], **Pierre Cordelier**[1], **Pierre Brousset**[1,4], **Philippe Rochaix**[1,4], **Sandrine Silvente-Poirot**[1,8], **Nicole Therville**[1], **Nathalie Andrieu-Abadie**[1,2], **Thierry Levade**[1,2,3,9], **Yusuf A. Hannun**[5], **Hervé Benoist**[1,2,3], **Nicolas Meyer**[1,4], **Olivier Micheau**[6,7], **Céline Colacios**[1,2,3], **Bruno Ségui**[1,2,3]

[1]INSERM UMR 1037, Cancer Research Center of Toulouse (CRCT), Toulouse, France.

Corresponding Author: Bruno Ségui, INSERM UMR1037, Cancer Research Center of Toulouse, 2 Avenue Hubert Curien, Toulouse Cedex 1 31037, France. Phone: 33582741621; bruno.segui@inserm.fr.

A. Montfort, F. Bertrand, and J. Rochotte share co-first authorship of this article.

C. Colacios and B. Ségui contributed equally as co-senior authors of this article.

Authors' Contributions

A. Montfort: Conceptualization, formal analysis, investigation, writing–original draft, writing–review and editing. **F. Bertrand:** Conceptualization, formal analysis, investigation. **J. Rochotte:** Conceptualization, formal analysis, investigation. **J. Gilhodes:** Formal analysis, methodology, writing–original draft. **T. Filleron:** Validation, methodology. **J. Milhès:** Investigation. **C. Dufau:** Investigation. **C. Imbert:** Investigation. **J. Riond:** Investigation. **M. Tosolini:** Investigation, methodology. **C.J. Clarke:** Investigation, writing–review and editing. **F. Dufour:** Investigation. **A.A. Constantinescu:** Investigation. **N. De França Junior:** Investigation. **V. Garcia:** Investigation. **M. Record:** Methodology. **P. Cordelier:** Methodology. **P. Brousset:** Methodology. **P. Rochaix:** Methodology. **S. Silvente-Poirot:** Methodology. **N. Therville:** Investigation. **N. Andrieu-Abadie:** Writing–original draft, writing–review and editing. **T. Levade:** Writing–original draft, writing–review and editing. **Y.A. Hannun:** Writing–original draft, writing–review and editing. **H. Benoist:** Writing–original draft. **N. Meyer:** Methodology, writing–original draft, writing–review and editing. **O. Micheau:** Investigation, methodology, writing–original draft. **C. Colacios:** Conceptualization, formal analysis, supervision, validation, investigation, writing–original draft, writing–review and editing. **B. Ségui:** Conceptualization, formal analysis, supervision, funding acquisition, validation, investigation, writing–original draft, writing–review and editing.

Authors' Disclosures

A. Montfort reports grants from Ligue contre le Cancer Régionale Midi-Pyrénées, Fondation de France, Ligue Nationale contre le Cancer, Rotary Toulouse Clubs, Fondation ARC, Cancéropôle Grand Sud-Ouest, Fondation Toulouse Cancer Santé, Prestige Grant award (Marie Curie Actions and Campus France), and TRANSCAN research program during the conduct of the study, as well as a patent for WO2017134116A1 pending. F. Bertrand reports a patent for WO2017134116A1 pending. V. Garcia reports grants from Ligue contre le Cancer Régionale Midi-Pyrénées, Fondation de France, Ligue Nationale contre le Cancer, Rotary Toulouse Clubs, Fondation ARC, Cancéropole Grand Sud-Ouest, Fondation Toulouse Cancer Santé, Prestige Grant award (Marie Curie Actions and Campus France), and TRANSCAN research program during the conduct of the study. N. Andrieu-Abadie reports grants from INSERM, Paul Sabatier University Toulouse III, Ligue Nationale contre le Cancer, Ligue Régionale contre le Cancer (Midi-Pyrénées), INSERM Transfert, Cancéropole Grand Sud-Ouest, Rotary Toulouse Clubs, Fondation Toulouse Cancer Santé, Fondation ARC, ERA-NET Transcan-2, and Fondation de France during the conduct of the study, as well as a patent for WO2017134116A1 pending. T. Levade reports grants from INSERM, Paul Sabatier University, Toulouse III, Ligue Nationale contre le Cancer, Ligue Regionale contre le Cancer (Midi-Pyrénées), INSERM Transfert, Canceropole Grand Sud-Ouest, Rotary Toulouse Clubs, Fondation Toulouse Cancer Sante, Fondation ARC, ERA-NET Transcan-2, and Fondation de France during the conduct of the study, as well as a patent for WO2017134116A1 pending. N. Meyer reports grants and personal fees from Bristol-Myers Squibb and MSD, and personal fees from Roche, Novartis, Pierre Fabre, Sanofi, Sun Pharma, and AbbVie outside the submitted work. O. Micheau reports grants from ANR, CAPES-COFECUB, and INCa during the conduct of the study. C. Colacios reports grants from INSERM, Paul Sabatier University, Toulouse III, Ligue Nationale contre le Cancer, Ligue Regionale contre le Cancer (Midi-Pyrénées), INSERM Transfert, Cancéropôle Grand Sud-Ouest, Rotary Toulouse Clubs, Fondation Toulouse Cancer Santé, Fondation ARC, ERA-NET Transcan-2, and Fondation de France during the conduct of the study, as well as a patent for WO2017134116A1 pending. B. Ségui reports grants from INSERM, Paul Sabatier University, Toulouse III, Ligue Nationale contre le Cancer, Ligue Régionale contre le Cancer (Midi-Pyrénées), INSERM Transfert, Cancéropôle Grand Sud-Ouest, Rotary Toulouse Clubs, Fondation Toulouse Cancer Santé, Fondation ARC, ERA-NET Transcan-2, and Fondation de France during the conduct of the study; grants and personal fees from Bristol-Myers Squibb outside the submitted work; and a patent for WO2017134116A1 pending. No disclosures were reported by the other authors.

Note: Supplementary data for this article are available at Cancer Immunology Research Online (http://cancerimmunolres.aacrjournals.org/).

[2]Equipe Labellisée Fondation ARC pour la recherche sur le cancer, Toulouse, France.

[3]Université Toulouse III - Paul Sabatier, Toulouse, France.

[4]Institut Universitaire du Cancer (IUCT-O), Toulouse, France.

[5]Stony Brook Cancer Center, and Department of Medicine, Stony Brook University, New York, New York.

[6]INSERM, UMR1231, Laboratoire d'Excellence LipSTIC, Dijon, France.

[7]UFR Sciences de Santé, Université Bourgogne Franche-Comté (UBFC), Dijon, France.

[8]Team "Cholesterol Metabolism and Therapeutic Innovations," Cancer Research Center of Toulouse (CRCT), UMR1037 Inserm/Université Toulouse III - Paul Sabatier/ERL5294 CNRS, Toulouse, France.

[9]Laboratoire de Biochimie, Institut Fédératif de Biologie, CHU Purpan, Toulouse, France.

Abstract

Dysregulation of lipid metabolism affects the behavior of cancer cells, but how this happens is not completely understood. Neutral sphingomyelinase 2 (nSMase2), encoded by *SMPD3*, catalyzes the breakdown of sphingomyelin to produce the anti-oncometabolite ceramide. We found that this enzyme was often downregulated in human metastatic melanoma, likely contributing to immune escape. Overexpression of nSMase2 in mouse melanoma reduced tumor growth in syngeneic wild-type but not CD8-deficient mice. In wild-type mice, nSMase2-overexpressing tumors showed accumulation of both ceramide and $CD8^+$ tumor-infiltrating lymphocytes, and this was associated with increased level of transcripts encoding IFNγ and CXCL9. Overexpressing the catalytically inactive nSMase2 failed to alter tumor growth, indicating that the deleterious effect nSMase2 has on melanoma growth depends on its enzymatic activity. *In vitro*, small extracellular vesicles from melanoma cells overexpressing wild-type nSMase2 augmented the expression of IL12, CXCL9, and CCL19 by bone marrow–derived dendritic cells, suggesting that melanoma nSMase2 triggers T helper 1 (Th1) polarization in the earliest stages of the immune response. Most importantly, overexpression of wild-type nSMase2 increased anti–PD-1 efficacy in murine models of melanoma and breast cancer, and this was associated with an enhanced Th1 response. Therefore, increasing *SMPD3* expression in melanoma may serve as an original therapeutic strategy to potentiate Th1 polarization and $CD8^+$ T-cell–dependent immune responses and overcome resistance to anti–PD-1.

Introduction

Sphingolipids (SL) are essential structural and signaling molecules able to modulate cell growth, differentiation, migration, and death as well as cancer progression (1). Ceramide is an important SL that behaves as an anti-oncometabolite (2). It can be generated by hydrolysis of sphingomyelin (SM) as a consequence of sphingomyelinase (SMase) activation (2). Several SMases have been described so far including neutral, alkaline, and acid SMases (3).

Among neutral SMases, neutral SMase 2 (nSMase2), which is encoded by *SMPD3* (4), is activated by an array of stimuli, including proinflammatory cytokines such as IL1β (5) and TNFα (6). Anthracyclines also increase transcription of *SMPD3* in MCF-7 breast cancer cells, a phenomenon able to promote cell growth arrest and cell death (7). In addition, overexpression of nSMase2 inhibits the growth of the F4328 mouse osteosarcoma cell line (8). Although the role played by nSMase2 in cancer progression remains to be fully addressed, inactivating *SMPD3* mutations are observed in some patients with acute myeloid or lymphoid leukemia (8), and *SMPD3* expression is downregulated in some human and mouse mammary tumors via epigenetic mechanisms (9).

Our group reported alterations of SL metabolism in melanoma (10-17). For instance, downregulation of *SGMS1*, the gene encoding sphingomyelin synthase 1, is associated with SL metabolism reprogramming in melanoma cells and a worse prognosis in patients with advanced melanoma (14). Other researchers have shown that β-galactosylceramidase (GALC) plays an oncogenic role in melanoma by limiting the expression of nSMase2 and ceramide levels (18). Conversely, GALC downregulation induces nSMase2 upregulation, with a subsequent increase of intracellular ceramide, and inhibits the tumorigenic activity of mouse and human melanoma cells (18).

Melanoma is a highly immunogenic cancer, the progression of which is associated with immune escape mechanisms. MAbs inhibiting immune checkpoints such as CTLA-4 and PD-1 have demonstrated significant efficacy in the treatment of metastatic melanoma, yielding high response rate and long-lasting tumor control. Despite promising results, about 40% of patients do not have therapeutic responses, and a significant proportion of responders experience tumor relapse within 2 years following treatment induction (19). To the best of our knowledge, whether melanoma nSMase2 influences immune responses and the response of tumors to immune checkpoint inhibitors (ICI) is currently unknown.

Herein, we investigated the role of nSMase2 in melanoma progression and its influence on the response of tumors to anti–PD-1 therapy. We found that *SMPD3* was frequently downregulated and mutated in patients with melanoma, likely contributing to immune escape mechanisms. We went on to demonstrate that correcting the expression of nSMase2 in mouse melanoma enhanced Th1 and $CD8^+$ T-cell–dependent immune responses and potentiated the efficacy of ICI therapy *in vivo*.

Materials and Methods

SMPD3 expression, mutations, and DNA methylation in human melanoma

SMPD3 expression in patients with primary and metastatic melanoma was evaluated using the Oncomine (20) and The Cancer Genome Atlas (TCGA) melanoma (21) databases; each dataset was evaluated separately (Fig. 1). TCGA genomic and clinical data were downloaded from the UCSC cancer genome browser project (http://www.genome.ucsc.edu/). Among the 422 patients with melanoma from the TCGA dataset, the analysis population consisted in 342 patients with distant metastasis for whom there were overlapping RNA sequencing and clinical data (Supplementary Data File S1). No other inclusion/exclusion criteria were applied for this analysis. Differentially expressed genes (DEG) in human metastatic

melanoma samples exhibiting high ($n = 68$) versus low ($n = 68$) *SMPD3* expression were identified according to a fold-change (FC) threshold of 2 and a P value < 0.05 adjusted with the Benjamini–Hochberg procedure. Voom transformation and DEG analysis were performed with R packages egdeR and limma, respectively. The top 200 genes upregulated (FC > 7.75) in human metastatic melanoma samples exhibiting high *SMPD3* expression level group were selected for pathway analysis. This was performed with Autocompare ZE based on the Zelen exact test for P value estimation (ref. 22; available at https://sites.google.com/site/fredsoftwares/products/autocompare-ze) using C5 database from the Broad Institute (http://software.broadinstitute.org/gsea/msigdb/collections.jsp; ref. 23). Date of origin for computation of overall survival was the date of specimen procurement. Survival rates were estimated using the Kaplan–Meier method, and comparison between groups (low expression vs. high expression) was performed using the log-rank test. The strength of relationship between continuous covariates was assessed using Spearman rank correlation coefficient. DNA methylation data, obtained with the Infinium HumanMethylation450K BeadChip technology, were available for 233 patients out of the 342 patients with metastatic melanoma and downloaded from TCGA website. *SMPD3* mutation analysis in human melanoma was assessed on cBioportal (http://www.cbioportal.org/; refs. 24,25). The characterization of mutations predicted to be potentially damaging for nSMase activity was assessed by polyphen2 (http://genetics.bwh.harvard.edu/pph2/).

Cell lines

B16K1 is a genetically modified cell line kindly provided by Dr. Anne Françoise Tilkin Mariamé in 2010 (26, 27). To generate the B16K1 cell line, B16F10 cells were engineered to stably express the MHC class I molecule H-2Kb (27). B16K1 cells were cultured in DMEM medium (Gibco, #61965-026) containing 10% heat-inactivated FCS and were authenticated in February 2012 by the Leibniz Institute DSMZ GmbH. To guarantee cell line authenticity, the B16K1 cell line was used within 10 passages following thawing and tested for the expression of melanocyte-lineage proteins such as tyrosinase-related protein 2 (TRP2). Medium was changed every 2 to 3 days. 4T1 cells were from the ATCC (CRL-2539) and kindly provided by Dr. F. Cabon (CRCT) in 2015; they were not further authenticated, used within a maximum of 10 passages from thawing, and cultured in DMEM medium containing 10% FCS. Yumm 1.7 cells were kindly provided by Dr. M. Bosenberg (Yale University School of Medicine, New Haven, CT) in 2014. Cells were generated from tumors of $Braf^{V600E}Cdkn2A^{-/-}Pten^{-/-}$ mice and were described elsewhere (28, 29). Yumm 1.7 cells were cultured in Opti-MEM (Gibco, #31985-047) supplemented with 5% FCS. Cell lines were tested for the absence of mycoplasma contamination by PCR using the GoTaq G2 DNA polymerase Kit (Promega, #M7845) and the primers: GCT GTG TGC CTA ATA CAT GCA T; ACC ATC TGT CAC TCT GTT AAC CTC.

Cell transfection

B16K1 cells were transfected (Superfect reagent, QIAGEN, #301305) with a plasmid (pEF6-V5-TOPO, Invitrogen, #46-0705) containing the cDNA encoding mouse nSMase2, which was kindly provided by Dr. Y. Hannun and was previously described (30). These transfected cells produce a V5-tagged nSMase2. Transfected cells were selected for their resistance to blasticidin (7 μg/mL; Invivogen, #ant-bl-1). Resistant cells were cultured in

DMEM containing 10% FCS and 7 μg/mL blasticidin, and analyzed by Western blot for the detection of the V5 tag (see below for Western Blot protocol). Two cell populations were selected: B16K1 nSMase2^{high} and B16K1 nSMase2^{low}, which overexpressed or not V5-tagged nSMase2, respectively. Mock-transfected B16K1 cells were obtained by transfecting a plasmid conferring resistance to blasticidin. nSMase enzyme activity was also assessed to determine nSMase2 overexpression (see below for protocol).

Mice

Wild-type (WT) C57BL/6 mice were from Janvier Laboratories. CD8α-deficient C57BL/6 mice were a gift from Prof. J. van Meerwijk (INSERM U1043, Toulouse, France). For each experimental condition, 6- to 12-week-old female mice were used. Mice were maintained in specific pathogen–free conditions at the CRCT animal facility (US006 CREFRE - Inserm/UPS), which is accredited by the French Ministry of Agriculture to perform experiments on live mice (accreditation number A-31 55508). All *in vivo* experimental protocols were conducted with the approved of the local ethic committee, an Institutional Animal Care and Use Committee, and in accordance with the French and European regulations on care and protection of Laboratory Animals.

In vitro bone marrow–derived dendritic cell culture

To generate mouse dendritic cell (DC) *in vitro*, bone marrow–derived cells (BMDC) from C57BL/6 mice were harvested and cultured in complete RPMI, which was RPMI (Gibco, #61870-010) supplemented with 10% FCS, penicillin (100 U/mL), streptomycin (100 μg/mL; Sigma, #P0781), 50 μmol/L β-mercaptoethanol (Gibco, #31350-010), and 20 ng/mL GMCSF (Peprotech, #315-03-100UG) at 37°C with 5% CO_2. At day 3, nonadherent cells were removed, and new complete RPMI was added with half of it changed every 2 to 3 days. After at least 7 days of culture, DC differentiation was analyzed by FACS as described below. DCs were cultured for 24 hours in the presence or absence of 5 to 10 μg/mL small extracellular vesicles (sEV), purified as described below.

sEV purification

sEV purification was performed as previously described from the conditioned medium of B16K1 nSMase 2 WT and catalytically inactive (C.I.) cells (31). Briefly, cells were cultured in DMEM 10% sEV-free FCS (prepared after overnight centrifugation at 100,000 × *g*, 4°C). The medium was collected after 3 days of culture, and sEVs were isolated by differential ultracentrifugation. Briefly, the culture medium was centrifuged at 300 × *g* for 10 minutes. The supernatant was then sequentially centrifuged at 2,000 x *g* for 20 minutes, at 10,000 x *g* for 45 minutes, and at 110,000 × *g* for 70 minutes at 4°C to sediment sEVs. The sEV pellet was then washed with PBS, and further centrifuged at 110,000 × *g* for 70 minutes at 4°C. The resultant sEV pellet was resuspended in PBS for *in vitro* culture and FACS analysis or in Western blot cell lysis buffer (see protocols below).

Western blot analysis

Cells and sEVs were lysed in a buffer containing 50 mmol/L HEPES (Sigma, #H3375), pH 7.5, 150 mmol/L NaCl (Sigma, # S-9625), 10% glycerol (Sigma, #G-7893),

1% Triton X-100 (Sigma, #X100), 1 mmol/L $NaVO_4$ (Sigma, #S-6508), 10 mmol/L β-glycerophosphate (Sigma, #G9891), 50 mmol/L NaF (Sigma, #S-7920), 1 mmol/Lphenylmethylsulfonyl fluoride (Sigma, #P-3075), 10 μg/mL leupeptin (Sigma, #L2884), 2 μg/mL pepstatin A (Sigma, #P-5318), and 10 μg/mL aprotinin (Sigma, #A6279) for 30 minutes on ice and sonicated. Equal amounts of proteins were separated in a 7.5% to 10% SDS-polyacrylamide gel and blotted onto nitrocellulose membranes (Hybond-C, Amersham Pharmacia Biotech, GE Healthcare, #10600002). Proteins were detected using anti-V5 (Invitrogen, #477701A) and anti–β-actin (Cell Signaling Technology), anti-mouse TRP2 (Santa Cruz Biotechnology, #sc-10451), anti-mouse TSG101 (Abcam, #ab83), anti-mouse HSP70 (Cell Signaling Technology, #4872), and anti-mouse, anti-goat, or anti-rabbit horseradish peroxidase–conjugated IgG (Cell Signaling Technology). Staining was revealed using an ECL detection system (Clarity Western ECL substrate, Bio-Rad, #170-5060) and visualized by film exposure (Genesee Scientific, #30-101) or Chemidoc Imaging systems (Bio-Rad).

In vitro PD-L1 expression

B16K1 cells (0.3×10^5) expressing high or low levels of nSMase2 were plated in 6-well plates and treated with vehicle [PBS (Eurobio Scientific, #CSP1PBS01-01)], 0.1% BSA (Euromedex, #1035-70-C), 50 ng/mL recombinant murine TNF (Peprotech,#315-01A), and 100 U of recombinant murine IFNγ (Peprotech, #315-05) alone or combined in DMEM 10% FCS for 72 hours. Cells were detached using Versene solution (Gibco, #15040-033), PD-L1 expression (BD Biosciences, MIH5) was assessed by flow cytometry on an LSRFortessa X-20 (BD Biosciences), and data were analyzed with the FlowJow10 software.

mRNA ISH

Biopsies of melanoma tumors were performed on five patients between 2014 and 2017. All patients provided informed written consent. No particular inclusion/exclusion criteria were applied. The protocol was approved by “CPP du Sud-Ouest et Outre-Mer IV” (Limoges, France) committee. Patient studies were performed in accordance to the Declaration of Helsinki. ISH for *SMPD3* mRNA was performed on formalin-fixed paraffin-embedded cutaneous tumor sections (and surrounding healthy tissue) using a specific probe from RNA ScopeVR (Advanced Cell Diagnostics, #490279) and the Ventana Discovery–automated ISH slide staining systems according to the manufacturer’s instructions.

Cloning WT and C.I. V5-nSMase2 in pMSCV-Puro

Retroviral expression vectors encoding WT or mutant (D428A) mouse nSMase-2 were obtained by cloning the product of the partial BamHI and PmeI digestion of pEF6-V5-His (Clontech, Takara, K1062-1) donor expression vectors encoding WT and C.I. mouse nSMase-2 into pMSCV-Puro (Clontech, #634401; ref. 32) linearized with BglII and HpaI.

Retrovirus production and cell transduction

The generation of retroviruses has been described previously (33). Viral particles of WT and C.I. (D428A) nSMase-2 derived from pMSCV-Puro vectors or control vector

(pMSCV-Puro empty vector) were produced to transduce 1 to 3 × 10^6 mouse B16K1, Yumm1.7, and 4T1 for 16 hours in 6-well plates in the presence of Polybrene (8 μg/mL, Santa Cruz Biotechnology, #134220) in DMEM 10% FCS. Cells were then washed in PBS, harvested, plated in DMEM 10% FCS containing puromycin (2.5 μg/mL, Gibco, #12122530), and incubated for 3 days before amplification and subsequent analysis of the polyclonal populations (puromycin selection, enzyme activity assay, and Western blot for detection of the V5 Tag as described in the sections above and below). B16K1 and 4T1 cells overexpressing the WT or C.I. form of nSMase2 are mentioned in the text as B16K1 nSMase2 WT or C.I. and 4T1 nSMase2 WT or C.I.; the Yumm1.7 transduced with the vector encoding WT nSMase2 or control vector are mentioned in the text as Yumm nSMase2 WT or control.

In vitro B16 melanoma cell proliferation and clonogenicity

To study cell proliferation, B16 cells were cultured in DMEM medium containing 0% or 10% FCS. Cells were counted at the indicated times using a cell counter (Beckman). Melanoma cells were grown on soft agar (clonogenicity assay) or as spheroids. For the growth on soft agar, 6-well plates were precoated with 2 mL DMEM 4.5 g/L glucose containing 10% FCS and 0.6% agar (Euromedex, #EU0031). DMEM (2 mL) containing 10% FCS, 0.3% agar, and 10,000 B16K1 nSMase2^{high} or nSMase2^{low} cells were overlaid onto the precoated wells. After a 2-week incubation at 37°C in 5% CO_2 atmosphere, cell colonies were visualized by 3-(4,5-dimethylthiazol-2-yl)-2,5-diphenyltetrazolium bromide (MTT) staining (500 μg/mL, Euromedex, #4022-B) at 0.5 mg/mL diluted DMEM 10% FCS and incubated at 37°C for 1 hour before washing with PBS and imaging (phase-contrast pictures, Olympus CKX41, Olympus Life Science). For spheroid growth, 96-well plates were precoated with 50 μL 1% agarose (Lonza, #50004). Three thousand B16K1 nSMase2^{high} or nSMase 2^{low} cells were overlaid onto the precoated wells in DMEM 4.5 g/L glucose (100 μL) containing 10% FCS. After a 12-day incubation at 37°C in 5% CO_2 atmosphere, spheroids were imaged using the Olympus CKX41 microscope (phase-contrast pictures).

Neutral SMase activity measurement

Cellular and tumor nSMase activities were assayed as described previously (34) using [choline-methyl-^{14}C]SM (100,000 dpm/assay) as substrate. Briefly, B16K1, Yumm1.7, and 4T1 cells were resuspended in a buffer containing 0.1% Triton X100 (Sigma, #X100), 20 mmol/L HEPES (pH 7.4; Sigma, #H3375), 10 mmol/L $MgCl_2$ (Euromedex, 2189-A), 2 mmol/L EDTA (Sigma, #E-5134), 5 mmol/L DTT (Euromedex, #EU0006-A), 0.1 mmol/L Na_3VO_4 (Sigma, #S-6508), 0.1 mmol/L Na_2MoO_4 (Sigma, #331058), 10 mmol/L β-glycerophosphate (Sigma, G9891), 750 μmol/L ATP (Sigma, #FLAAS), 10 μmol/L leupeptine (Sigma, #L2884), and 10 μmol/L pepstatin-A (Sigma, #P-5318) and sonicated. For tumors, 1 mL of the above-mentioned buffer was used to homogenize 100 mg of tumor extract using the FastPrep 24 technology (MP Biomedical) with ceramic beads (MP Biomedicals, #6913100). nSMase activity assay was performed by mixing the protein extract with [choline-methyl-^{14}C]SM [100,000 dpm/assay; PerkinElmer, NEC6630 (IOUC)] resuspended in a buffer containing 20 mmol/L HEPES (pH 7.4) and 1 mmol/L $MgCl_2$ as substrate (v/v) for 2 hour at 37°C. The generated [^{14}C] phosphorylcholine is then separated

by Floch technique by adding chloroform/methanol (2:1, v/v) solution and counting of the radioactive aqueous phase by scintillation on the Tri Carb 2910 TR (Perkin Elmer) using the liquid scintillation cocktail Ultima Gold (Perkin Elmer, #6013329).

SL analysis from tumors

Tumors were collected and homogenized in 20 mm Tris buffer with protease inhibitors (Roche, #11873580001) using glass beads (Sigma Aldrich, #G8772) in the FastPREP-24 Classic instrument (MP Biomedicals). Lipids were initially extracted from 0.5 to 1 mg of tumor cell lysate by addition of 2 mL 2:3 70% isopropanol:ethyl acetate and submitted for analysis at Stony Brook Lipidomics core. Lipids were further extracted by addition of 2 mL 2:3 70% isopropanol:ethyl acetate and centrifugated for 5 minutes (1,000 x *g*). Organic phases were dried down and reconstituted in 100 μL mobile phase B (0.2% formic acid, 1 mmol/L ammonium formate in methanol). SL analysis was carried out by tandem high-performance liquid chromatography: mass spectrometry on a Thermo Finnigan TSQ 7000 triple quadrupole mass (35). Ceramide peaks were identified by comparison with known standards, and the area under the curve was measured. Absolute lipid levels were determined using a standard curve of known lipid amounts using standards. Results from mass spectrometry analysis were normalized to total protein concentration as determined by Bradford assay (Bio-Rad, #500-0006).

RNA isolation and qRT-PCR

For RNA isolation from tumors 12 days after B16K1 cell injection, tumors were collected and dissociated using a tissue homogenizer (Precellys, Bertin) using at 6,500 rpm for 2 cycles of 30 seconds in vials containing ceramic beads (MP Biomedicals, #6913100). RNA was purified using the RNeasy Midi Kit (QIAGEN, #75144). cDNA from total RNA was prepared with the Superscript II Reverse Transcriptase using 1 μg of RNA from each sample (Thermo Fisher Scientific, #18064022). qPCR was performed using the SYBR Green Master Mix (Takara, #RR420L) and primers for transcripts encoding murine β-actin (QT01136772), hypoxanthine-guanine phosphoribosyltransferase (HPRT; QT00166768), CXCL9 (QT00097062), IL12p40 (QT00153643), CCL19 (QT02532173), CCL2 (QT00167832), CXCL11 (QT00265041), CXCL10 (QT00093436), CCL5 (QT01747165), TNF (QT00104006), CCL17 (QT00131572), CCL22 (QT00108031), and IL1β (QT01048355; QIAGEN, QuantiTech Primer Assay). Assays were run on the StepOne Plus instrument (Thermo Fisher Scientific), and gene expression for all cytokines and chemokines tested was calculated according to the formula $2^{-\Delta Ct}$. The mean Ct value for the expression level of HPRT and β-actin was used as reference.

Confocal microscopy analysis

B16K1 cells were cultured on glass coverslips for 24 hours and fixed in PBS paraformaldehyde. Cells were stained with anti-giantin (Invitrogen, #BS-13356R) and anti-V5 (Invitrogen, #2F11F7) antibodies and dye-coupled secondary antibodies [goat anti-rabbit IgG Alexa Fluor 488 (Invitrogen, #A11008); goat anti-mouse IgG2a Alexa Fluor 568 (Invitrogen, #A-21134)] and analyzed by confocal microscopy (Zeiss, LSM510).

In vivo tumorigenesis of B16K1 cells

B16K1 cells (3×10^5) expressing WT or C.I. V5-tagged nSMase2 were intradermally injected in WT or CD8α-deficient mice. Tumor volume was calculated using a caliper at the indicated days with the formula: Tumor volume = $0.52 \times \text{length} \times \text{width}^2$. For some experiments, mice received i.p. injection of anti–PD-1 therapy (200 μg; BioXcell; clone RMP1-14), anti–CTLA-4 (200 μg first cycle then 100 μg; BioXcell; clone 9H10), or vehicle (PBS) on days 6, 10, and 13 after tumor cell injection.

Tumor immune infiltrate analysis

One million B16K1 cells overexpressing or not a WT or C.I. V5-tagged nSMase2 were intradermally and bilaterally injected in WT mice. Tumors were weighed and digested with the mouse Tumor Dissociation Kit (Miltenyi, #130-096-730) before flow cytometry analysis.

Flow cytometry analyses

For the analysis of sEVs by flow cytometry, 4 μL of latex beads (Invitrogen, #A37304) diluted in 1 mL PBS were precoated with 5 μg of sEVs during 16 hours at 4°C under rotation. Following BSA (Euromedex, #1035-70-C) saturation and washing, beads were incubated with an anti-mouse CD63 (BioLegend, NVG-2).

To analyze for the *in vitro* maturation of DCs, cells were cultured with or without 10 μg/mL sEVs during 24 hours and then stained with the following antibodies: anti-CD11c (eBioscience, N418), anti-CD80 (eBioscience, 16-10A1), anti-CD86 (BB Biosciences, PO3), anti–MHC-I (BD Biosciences, AF6-88.5), and anti–MHC-II (eBioscience, M5/114.15.2).

For the analysis of the tumor immune infiltrate, cells were stained with antibodies or MHC-I/TRP2 dextramers (APC-conjugated H-2Kb/SVYDFFVWL, Immudex) and live-dead reagents (Invitrogen, #L34TIL analysis). To assess for IFNγ and TNF production by tumor-infiltrating lymphocytes (TIL), cells from the dissociated tumors were incubated for 4 hours in the presence of 1X cell stimulation cocktail (eBioscience, #00-4970-93) and 1X Protein transport inhibitor (eBioscience, #00-4980-03) prior to cytometry analysis. Antibodies used in this study were as follows: anti-mouse CD45 (BD Biosciences, 30-F11), anti-mouse Thy1.1 (BioLegend, H12), anti-mouse CD8 (BioLegend, 53-6.7), anti-mouse CD4 (BD Bioscience, GK1.5), anti-mouse FoxP3 (eBioscience, FJK-16s), anti-mouse CD11c (eBioscience, N418), anti–PD-L1 (BD Bioscience, MIH5), anti-IFNγ (BD Biosciences, XMG1.2), anti-TNF (BD Biosciences, MP6-XT22), anti-Granzyme B (BioLegend, GB11), anti–TIM-3 (eBioscience, J43), anti–CTLA-4 (eBioscience, UC10), and anti-TCRβ (BD Bioscience, H57–597). For the staining of intracellular targets, cells were first stained for membrane markers, then fixed and permeabilized using the “Foxp3 fixation/permeabilization staining buffer set” (eBioscience, #00-5523-00) before staining for Foxp3 or TNF and IFNγ. Samples were acquired using an LSRFortessa X-20 (BD Biosciences), and data were analyzed with the Diva or FloJow 10 softwares. Gating strategies are depicted in Supplementary Data File S2.

Statistical analysis

Each experiment was designed to use the minimum number of mice or samples required to obtain informative results and sufficient material for subsequent studies. No specific statistical tests were used to predetermine the sample size. For animal experimentation, we used at least 5 mice per group, and experiments were typically performed twice, unless otherwise stated in the figure legends. Statistical significance of difference between groups was evaluated using the GraphPad Prism 7 software. Briefly, we tested whether the values come from a Gaussian distribution using a D'Agostino–Pearson omnibus normality test. When passing the normality test, a Student *t* test was used. Otherwise, a Mann–Whitney *U* test was used. For statistical significance of animal survival, the log-rank test was used. Differences were considered to be statistically significant when $P < 0.05$ (*, $P < 0.05$; **, $P < 0.01$; ***, $P < 0.001$). *In vivo* and *in vitro* experiments were monitored in a nonblinded fashion, and no method of randomization was used. In tumorigenesis experiments, mice for which no tumor was observed during 10 days after the inoculation of cancer cells were excluded. For the analysis of TILs, tumors in which the number of cells was too small were excluded from the analysis.

Results

SMPD3 expression in human melanoma biopsies correlates with a $CD8^+$ T-cell gene signature

Analysis from the Oncomine database indicated that low levels of *SMPD3* transcripts are found in human metastatic melanoma as compared with primary tumors and normal skin (Fig. 1A), suggesting that nSMase2 downregulation is likely associated with melanoma progression. ISH experiments on skin sections from patients with advanced melanoma using RNAscope technology revealed robust and low *SMPD3* expression in the tumor-adjacent stratum granulosum and cutaneous melanoma, respectively (Fig. 1B; Supplementary Fig. S1A-S1D). Moreover, a majority of tumor biopsies from the TCGA cohort of patients with advanced melanoma expressed *SMPD3* at low levels (Fig. 1C). Because gene hypermethylation has been shown to downregulate *SMPD3* expression in solid tumors (9), we analyzed the methylation status of *SMPD3* in the TCGA melanoma cohort. This analysis identified one CpG island located within the promoter core (73 pb downstream of the transcription start site) for which the methylation level (>0.27) inversely correlated to gene expression (Supplementary Fig. S1E and S1F). This suggests that, at least in some patients, DNA methylation of the promoter region may contribute to *SMPD3* downregulation in melanoma. The clinical outcome for patients with metastatic melanoma exhibiting high and low *SMPD3* expression was analyzed. Low *SMPD3* expression was significantly associated with shortened overall survival (Fig. 1D), further suggesting that *SMPD3* downregulation is associated with a worse prognosis for patients with melanoma.

Focusing on the TCGA melanoma cohort, we examined which gene signatures were associated to high or low levels of *SMPD3* expression in tumor samples. A high *SMPD3* expression was mostly associated with signatures related to "Immune system process" and "Lymphocyte activation" according to Gene ontology classification (Supplementary Table S1). Further analysis showed that high *SMPD3* expression was associated with high

expression of *CD3G, CD3D*, and *CD3E*, which reflect TILs (Fig. 1E; Table 1). Among T-cell–associated genes, we found that *CD8A, CD8B*, and *CD4* were enriched in melanoma samples expressing *SMPD3* at high levels. Moreover, various Th1-related genes such as *IL12, CXCL10*, and *TBX21* as well as genes related to cell-mediated cytotoxicity were expressed at higher levels in melanoma samples exhibiting high *SMPD3* expression (Fig. 1E; Table 1). Accordingly, *SMPD3* expression significantly correlated with the expression of a set of genes, which likely reflect $CD8^+$ T-cell infiltration (Fig. 1F; Table 1). The expression level of genes encoding other known SMases was not associated with a gene signature of $CD8^+$ TILs in patients with metastatic melanoma except for *SMPD2*, which poorly, yet significantly, correlated with *CD8B* (Table 1). In contrast, *SMPD4* was negatively correlated with T-cell–related genes (Table 1).

Thus, expression of *SMPD3* (but not the expression of other SMases) is associated with a $CD8^+$ T-cell gene signature in human melnoma samples. We hypothesize that this may contribute to the improved overall survival seen for patients with high *SMPD3* expression.

nSMase2 expression impairs melanoma growth by enhancing $CD8^+$ T-cell responses

To assess the impact of *SMPD3* expression on melanoma growth and $CD8^+$ T-cell–mediated antitumor responses, we conducted studies using the B16K1 mouse melanoma cell line, which exhibits low endogenous nSMase activity (Supplementary Fig. S2A) and overexpresses MHC class I (26, 36). We first generated B16K1 melanoma cell lines with or without nSMase2 overexpression (Fig. 2A; Supplementary Fig. S2B). The overexpressed enzyme was mainly localized at the plasma membrane (Fig. 2B), and high expression of nSMase2 led to robust increases in cellular nSMase activity (Supplementary Fig. S2A) and ceramide levels (Fig. 2C), affecting neither two- nor three-dimensional cell growth nor clonogenicity *in vitro* (Supplementary Fig. S2C and S2D).

Upon intradermal injection of B16K1 cells in C57BL/6 mice, nSMase2 overexpression, as evaluated by Western blot (Supplementary Fig. S2E, top plot, and S2F), triggered an intratumor increase in nSMase activity (Supplementary Fig. S2E, bottom plot) and elevation of ceramide levels (Fig. 2D). More precisely, high nSMase2 expression led to increased levels of the C12, C14, C16, C18:1, C22:1, and C24:1 ceramides species in tumors (Fig. 2D). Of note, nSMase2 overexpression was also linked to a significant increase in intratumor sphingosine levels, but it did not significantly affect levels of SM and sphingosine 1-phosphate (S1P; Supplementary Fig. S2G). In addition, high nSMase2 expression was associated with a strong decrease in B16K1 tumor growth in WT mice, as compared with tumors expressing low levels of the enzyme (Fig. 2E).

Because nSMase2 overexpression did not decrease *in vitro* proliferation of B16K1 cells but impaired tumor growth *in vivo*, we hypothesized that high nSMase2 expression in melanoma cells could trigger a remodeling of the tumor microenvironment. Building upon the data obtained using human samples from the TCGA dataset, we analyzed the immune response in mice engrafted with B16K1 melanoma cells expressing nSMase2 at low or high levels. Leukocytes ($CD45^+$) and T cells ($Thy1^+$) frequencies were significantly increased in melanomas that expressed nSMase2 at high levels (Fig. 2F). Among T cells, the proportion

of $CD8^+$ TILs was 3-fold higher in tumors expressing nSMase2 at high levels than in tumors expressing low levels of the enzyme (Fig. 2F).

To determine whether this increase in $CD8^+$ TILs may be important in mediating the deleterious impact of nSMase2 on melanoma growth, $nSMase2^{high}$ and $nSMase2^{low}$ B16K1 cells were engrafted in CD8α-deficient mice. Importantly, high nSMase2 expression failed to impair B16K1 melanoma growth in CD8α-deficient mice (Fig. 2G).

Collectively, these data indicate that nSMase2 overexpression in mouse melanoma enhances $CD8^+$ T-cell–dependent immunity, which consequently impairs tumor growth.

nSMase2 enzyme activity is required for enhancing T-cell–dependent anti-melanoma immune responses

Our analysis of the *SMPD3* nucleotide sequence in human melanoma from four independent studies identified mutations in the coding sequence, ranging from 2.5% to 20% mutation frequency depending on the study (37-40). The highest mutation frequency was observed in desmoplastic melanoma, whereas the lowest was in uveal melanoma (Fig. 3A). Most of the mutations were missense mutations, and half of them affected residues in the catalytic domain (Fig. 3B). Moreover, 12 mutations were predicted to be potentially damaging for nSMase activity (HumDiv score > 0.85) according to PolyPhen-2 analysis (Fig. 3B).

We then evaluated whether a single missense mutation (D428A) in the catalytic domain of murine nSMase2, which potently impairs enzyme activity (41), had an impact on $CD8^+$ T-cell–dependent immune responses and melanoma growth in mice. B16K1 cells were transduced with a retroviral vector encoding either the WT or C.I. form of the V5-tagged nSMase2 (Supplementary Fig. S3A). This approach resulted in a significant increase in nSMase activity in WT nSMase2–expressing cells compared with mock-transduced cells (Supplementary Fig. S3B) but not in the ones expressing C.I. nSMase2. There were no differences in proliferation capacity *in vitro* (Supplementary Fig. S3C) or subcellular localization (Supplementary Fig. S3D) between the cells transduced with WT nSMase2 and those transduced with C.I. nSMase2. However, nSMase activity in WT nSMase2–transduced B16K1 cells, triggered by the retroviral LTR promoter, is less than the activity observed in $nSMase2^{high}$ B16K1 cells transfected with the pEF6-V5_TOPO plasmid, which has a strong promoter (EF-1α; Supplementary Fig. S3E). The *in vivo* growth of tumors retrovirally transduced to express WT nSMase2 was reduced (by more than 50%) as compared with mock-transduced B16K1 tumors, but overexpressing the C.I. nSMase2 failed to alter tumor growth (Fig. 3C). This indicates that the deleterious effect nSMase2 has on melanoma growth depends on its enzymatic activity.

Next, the immune response was analyzed at day 12 post-B16K1 cell injection, at the inflection point of growth curves. At this time point, WT nSMase2 tumor weight was already significantly reduced compared with C.I. nSMase2 tumor weight (Fig. 3D). In accordance with results displayed in Fig. 2, tumors expressing WT nSMase2 had higher levels of total $CD4^+$ and $CD8^+$ T cells in both tumor-draining lymph nodes and tumors compared with tumors expressing C.I. nSMase2 (Fig. 3E). We next analyzed the infiltration of tumors by $CD8^+$ T cells specific for TRP2, a differentiation antigen of melanocytic cells.

We observed higher proportions of TRP2-specific $CD8^+$ T cells in tumors expressing WT nSMase2 than in those expressing the C.I. enzyme (Fig. 3F).

Together, these data indicate that the catalytic activity of nSMase2 is required for enhancing T-cell–dependent immune responses toward melanoma cells.

nSMase2 enhances the expression of Th1-related cytokines

To get insights into the molecular mechanisms by which melanoma nSMase2 enhances $CD8^+$ T-cell–dependent immune responses, we first evaluated the impact nSMase2 has on the expression of Th1-related cytokines in tumors. We observed that the levels of mRNA encoding CXCL9 and IFNγ were significantly increased upon WT nSMase2 expression in melanoma tumors as compared with the ones expressing C.I. nSMase2 (Fig. 4A). Consistent with this, *SMPD3* expression was significantly correlated with the expression of *IFNG* and *CXCL9* genes in human melanoma biopsies (Fig. 4B).

nSMase2 facilitates the budding of exosomes, a subset of sEVs (42), and this likely contributes to the modulation of the anti-melanoma immune response (43-45). Accordingly, we purified and analyzed the molecular composition of sEVs secreted by B16K1 cell expressing WT and C.I. nSMase2 (Supplementary Fig. S4). The total amount of secreted sEVs (Supplementary Fig. S4A), the ultrastructural morphology of sEVs (Supplementary Fig. S4B), and the expression of in sEV markers (CD63, TSG101, and HSP70) and melanoma antigens (MC1R and TRP2; Supplementary Fig. S4C-S4E) were similar for both cell types. Considering that DCs efficiently take up sEVs, a phenomenon that can influence their phenotype (43), the ability of the sEVs to facilitate DC maturation *in vitro* was examined. The DC surface maturation markers CD80, CD86, MHC-I, and MHC-II were similarly upregulated upon incubation with sEVs from B16K1 expressing either WT or C.I. nSMase2 (Supplementary Fig. S4F). However, sEVs from B16K1-expressingWT nSMase2 greatly enhanced BMDC intracellular levels of mRNA encoding some Th1-related cytokines, namely IL12, CXCL9, and CCL19 (Fig. 4C and D). No significant changes were observed in the induction of other Th1-related cytokines such as CCL5, CXCL11, CXCL10, or TNF in BMDCs in response to sEVs from B16K1 nSMase2 WT or C.I. (Fig. 4E, top plots). Finally, we did not observe differences in the expression of transcripts encoding the myeloid chemoattractant CCL2, the regulatory T cell (Treg) chemoattractants CCL17 and CCL22, or the proinflammatory cytokine IL1β (Fig. 4E, bottom plots).

Collectively, the data indicate that melanoma nSMase2 enhances the expression of a set of Th1-related cytokines and chemokines in murine and human tumors, which likely facilitates the establishment of a $CD8^+$ T-cell–dependent immune response against melanoma.

nSMase2 expression in cancer cells enhances the efficacy of anti–PD-1 therapy in mice

nSMase2 overexpression significantly reduced B16K1 tumor growth in a $CD8^+$ T-cell–dependent manner but failed to trigger complete tumor rejection. Thus, we evaluated the impact of melanoma nSMase2 on the response to anti–PD-1 therapy, which is a gold standard in melanoma immunotherapy (19). We first evaluated the therapeutic activity of anti–PD-1 toward melanoma tumors expressing nSMase2 at low and high levels (Fig. 5A). Although anti–PD-1 therapy significantly delayed the growth of $nSMase2^{low}$ melanoma

(Fig. 5B and C), all tumors relapsed, presumably due to immune escape mechanisms and, consequently, all mice died within 40 days post-B16K1 injection (Fig. 5D). nSMase2 overexpression alone delayed melanoma growth (Fig. 5B and C) and significantly increased the overall survival (Fig. 5D). Strikingly, the therapeutic efficacy of anti–PD-1 therapy was dramatically enhanced by nSMase2 overexpression (Fig. 5B and C). In the group of mice injected with B16K1 nSMase2^{high} cells and anti–PD-1, all mice survived (Fig. 5D). Two months after the first tumor challenge, parental B16K1 melanoma cell reinjection in the surviving mice did not lead to tumor development and, as a consequence, did not compromise overall survival. This demonstrates that animals were totally vaccinated toward B16K1 melanoma cells (Fig. 5D).

We obtained similar results using the B16K1 tumor model comparing cells expressing WT or C.I nSMase2. WT nSMase2 significantly promoted the therapeutic efficacy of not only anti–PD-1 therapy but also anti–CTLA-4 therapy, whereas C.I. nSMase2 failed to do so (Supplementary Fig. S5A-S5C). Therefore, nSMase2 enzyme activity was required for enhancing ICI therapeutic efficacy. In this model, the effect obtained upon anti–PD-1 treatment was weaker than the one observed in Fig. 5. This difference might be related to the fact that B16K1 cells retrovirally transduced with WT nSMase2 exhibited significantly less nSMase activity than the B16K1-transfected cells (nSMase2^{high}; Supplementary Fig. S3E).

We confirmed the deleterious impact nSMase2 has on melanoma growth using another model, the Yumm 1.7 melanoma cells transduced with a control retroviral vector or a vector encoding for WT nSMase2 (Supplementary Fig. S6A). Overexpression of nSMase2 did not impair the *in vitro* proliferation of Yumm 1.7 cells despite increased nSMase activity, as compared with mock-infected cells (Supplementary Fig. S6A). However, nSMase2 overexpression not only dramatically impaired the growth of Yumm 1.7 tumors in immunocompetent mice, but also significantly reduced their resistance to anti–PD-1 therapy (Supplementary Fig. S6B).

To extend our observations to another cancer model and in a different mouse strain (BALB/c), we performed similar experiments using 4T1 breast cancer cells. Overexpressing WT nSMase2 in 4T1 cells significantly increased nSMase activity but did not compromise *in vitro* cell proliferation as compared with 4T1 cells overexpressing the C.I. nSMase2 (Supplementary Fig. S6C). However, WT nSMase2 slightly reduced the growth of 4T1 tumors in immunocompetent mice (Supplementary Fig. S6D). Anti–PD-1 therapy further reduced tumor growth in 4T1 tumors that overexpressed WT nSMase2, whereas C.I. nSMase2–overexpressing 4T1 tumors were totally resistant to anti–PD-1 therapy under our experimental conditions (Supplementary Fig. S6D).

Taken together, these data indicate that expression of WT nSMase2 in cancer cells enhances the efficacy of ICI in preclinical models.

nSMase2 expression enhances Th1 responses after anti–PD-1 therapy *in vivo*

To understand how melanoma nSMase2 enhanced the response to anti–PD-1 therapy, we monitored the immune response upon nSMase2 expression with or without anti–PD-1 therapy. nSMase2 overexpression increased the proportion of CD8$^+$ T cells in tumors (Fig.

6A) and decreased the proportion of $CD4^+Foxp3^+$ cells (i.e., Tregs) among $Thy1^+$ TILs (Fig. 6B and C), irrespective of anti–PD-1 therapy. In addition, nSMase2 overexpression increased the proportion of $CD4^+$ and $CD8^+$ TILs producing IFNγ and TNF, and this was further enhanced upon anti–PD-1 therapy (Fig. 6D and E). Of note, the proportion of $CD8^+$ TILs expressing granzyme B was significantly increased in B16K1 $nSMase2^{high}$ tumors under anti–PD-1 therapy (Fig. 6E). Considering the key role of IFNγ and TNF on PD-L1 expression (36,46,47), which can be a predictive marker of response to anti–PD-1 therapy, we next analyzed the expression of PD-L1 on macrophages ($CD11b^+F4/80^+$ cells), $CD45^-$ cells, and $CD11c^+$ DCs in tumors. We found that both nSMase2 overexpression and anti–PD-1 therapy increased PD-L1 expression on macrophages and $CD45^-$ cells. Combining nSMase2 expression and anti–PD-1 therapy further increased the expression of PD-L1, especially on $CD45^-$ cells (Supplementary Fig. S7A). The expression of PD-L1 on DCs was however increased only upon anti–PD-1 therapy in tumors expressing high levels of nSMase2 (Supplementary Fig. S7A). Of note, the upregulation of PD-L1 was unlikely a direct consequence of nSMase2 overexpression in melanoma cells because PD-L1 was not upregulated in nSMase2-overexpressing cells as compared with control cells *in vitro* (Supplementary Fig. S7B). Moreover, PD-L1 was equally upregulated on B16K1 cells expressing high or low levels of nSMase2 when treated with IFNγ alone or in combination with TNF *in vitro* (Supplementary Fig. S7B).

Finally, we observed no major impact of nSMase2 overexpression and/or anti–PD-1 treatment on the expression of TIM-3 and PD-1 on $CD4^+$ and $CD8^+$ TILs. We only observed a slight decrease in the percentage of $PD\text{-}1^+$ and $PD\text{-}1^+TIM\text{-}3^+$ $CD4^+$ TILs in $nSMase2^{high}$ tumors (Supplementary Fig S7C). We also observed a significant increase in CTLA-4 expression on $CD8^+$ TILs from $nSMase2^{high}$ tumors as compared with $nSMase2^{low}$ tumors, a phenomenon that was abrogated upon anti–PD-1 treatment (Supplementary Fig S7C).

Collectively, the data indicate that melanoma nSMase2 enhances Th1 responses upon anti–PD-1 therapy, thus facilitating tumor rejection.

Discussion

The present study provides the evidence that (i) *SMPD3* is expressed at low levels in most human metastatic melanoma samples and (ii) low *SMPD3* expression is associated with shortened overall survival in patients. High *SMPD3* expression was associated with "Immune system process" and "Lymphocyte activation" gene signatures, and melanoma samples expressing *SMPD3* at high levels exhibited a gene signature of TILs. In agreement with the data obtained from human melanoma databases, high nSMase2 expression increased $CD8^+$ TIL frequency and the $CD8^+$ T-cell–dependent immune response to decrease melanoma growth in WT mice but not in mice lacking $CD8^+$ T cells. This demonstrates that nSMase2 antitumorigenic properties are fully dependent on its ability to stimulate adaptive immunity. Collectively, our data reveal that *SMPD3* downregulation or mutation facilitates melanoma progression by contributing to melanoma immune escape.

The expression of genes encoding other SMase isoforms did not correlate with immune-related gene signatures in human melanoma. Thus, the distinctive biological properties of

nSMase2 in melanoma do not extend to the other SMases, presumably due to different subcellular localization and/or biochemical properties as well as different roles in cell signaling (48). One should note however that acid SMase likely modulates melanoma progression. Indeed, the growth of B16F1 melanoma cells is potentiated in acid SMase–deficient mice, indicating that the acid SMase–dependent pathway plays some critical role in the melanoma microenvironment (49), possibly by modulating tumor angiogenesis rather than the anti-melanoma immune response (50). In contrast, acid SMase deficiency in the host impaired melanoma cell metastasis. Mechanistically, acid SMase secretion by platelets has been proposed to trigger the activation of α5β1 integrins on B16F10 melanoma cells, thereby promoting melanoma cell extravasation to the lungs (51). Furthermore, acid SMase expression in human and mouse melanoma cells enhanced the proteasomal degradation of the microphthalmia-associated transcription factor (MITF; ref. 52). Consequently, acid SMase may limit the expression of key proteins involved in melanoma progression, which are regulated by MITF (52). More recently, melanoma acid SMase was shown to enhance the anti-melanoma immune response in mice, yet the molecular mechanisms remain to be established (53). We show that in human melanoma, the expression of *SMPD1*, the gene encoding acid SMase, did not correlate with the expression of diverse immune-related genes such as *CD8A* and *CD8B*, arguing against a role of acid SMase in $CD8^+$ T-cell–dependent immune responses in human melanoma.

The mechanisms by which nSMase2 facilitates the $CD8^+$ T-cell–dependent immune response likely rely on the alteration of intratumoral SL content because expression of a C.I. nSMase2 mutant had no effect on B16K1 tumor growth. Indeed, intratumoral ceramide and sphingosine content was increased in WT nSMase2–overexpressing melanoma tumors. Sphingosine is also a substrate of sphingosine kinases, which produce S1P, itself a critical mediator of lymphocyte trafficking (54). However, given that the levels of intratumor S1P remained unchanged upon nSMase2 overexpression, it is unlikely that S1P directly mediates the nSMase2-triggered increase in $CD8^+$ TILs. Another interesting hypothesis is that ceramide, which exhibits structural similarities to Lipid A, the biologically active core of lipopolysaccharide (55), may mimic pathogen-associated molecular patterns, facilitating DC maturation and ultimately priming the adaptive immune response. Recently, the administration of nanoliposome-loaded C6 ceramide in mice was shown to impair hepatocarcinoma growth by increasing M1 tumor-associated macrophage polarization and $CD8^+$ T-cell activation (56). While our study was in progress, nSMase2 expression was found to be inversely correlated with GALC during melanoma progression (18). This indicates that SM metabolism is tightly connected with that of glycosphingolipids, which are known to modulate the immune responses (57). Whether and how nSMase2 is a key player in mediating SM and glycosphingolipid relationships for modulating immune responses in melanoma remains to be investigated.

Under our experimental conditions, melanoma nSMase2 not only facilitated the Th1 polarization of TILs but also reduced the proportion of Tregs in tumors. Given that sEVs produced by B16K1 expressing WT nSMase2 promoted the expression of IL12, CXCL9, and CCL19 by DCs *in vitro*, this phenomenon might be implicated in the promotion of Th1 polarization *in vivo* and indicates that melanoma nSMase2 may trigger this polarization in the earliest stages of the immune response. Whereas nSMase2 overexpression in mouse

melanoma significantly delayed melanoma growth, all mice died within 40 days after melanoma cell injection, strongly suggesting melanoma immune escape. This is likely related to the increased expression of PD-L1 on both $CD11b^{+}F4/80^{+}$ macrophages and $CD45^{-}$ cells in B16K1 tumors overexpressing nSMase2. The latter phenomenon is likely the direct consequence of the nSMase2-dependent increased production of IFNγ and TNF in tumors (36, 46, 47). As a matter of fact, whereas anti–PD-1 therapy had limited therapeutic effects toward B16K1 melanoma, it greatly suppressed the growth of tumors overexpressing WT nSMase2. These observations demonstrate that melanoma nSMase2 enhances the therapeutic response to anti–PD-1 therapy. In addition, this enhanced therapeutic effect triggered by nSMase2 expression was also observed in Yumm 1.7 melanoma and 4T1 breast cancer cell lines, which are both resistant to anti–PD-1 therapy.

We previously demonstrated that increased expression of sphingosine kinase 1 by melanoma cells potently impairs $CD8^{+}$ T-cell–dependent immune responses and response to ICI (15). Our present study showing the positive impact *SMPD3* that has on antimelanoma immune responses further argues that targeting SL metabolism may represent an original therapeutic strategy to overcome resistance of melanoma to anti–PD-1 therapy. In addition, *SMPD3* expression in melanoma samples may serve as a novel biomarker to predict the clinical response to immunotherapy. This is currently being evaluated in a prospective clinical trial (IMMUSPHINX: NCT03627026) conducted in our institute and others, and the primary objective of this clinical trial is to evaluate whether SL metabolites and/or SL-metabolizing enzymes are putative biomarkers to predict response/resistance in patients with advanced melanoma treated with anti–PD-1 therapy alone or in combination with anti–CTLA-4 therapy.

Supplementary Material

Refer to Web version on PubMed Central for supplementary material.

Acknowledgments

The authors are grateful to the flow cytometry, microscopy, and animal facilities of the I2MC (INSERM U1048, Toulouse, France) and CRCT (INSERM U1037, Toulouse, France) for their technical assistance. They thank Drs. F. Sabourdy and S. Carpentier (INSERM U1037, Toulouse, France) for performing mutation analysis and technical assistance, respectively. They also thank Prof. J. van Meerwijk (INSERM U1043, Toulouse, France) for the kind gift of CD8-deficient mice. They also thank Prof. L. Nieto (IPBS, Toulouse, France) for sEVs analysis. They thank Drs. V. Douin-Echinard (INSERM U1048, Toulouse, France), J.C. Guéry (INSERM U1043, Toulouse, France), J. Torrisani, J.J. Fournié, L. Martinet, and A.F. Tilkin-Mariamé (INSERM U1037, Toulouse, France) for fruitful discussion.

This work was supported by INSERM, Paul Sabatier University (Toulouse III), Ligue Nationale contre le Cancer (LNCC, Equipe Labellisée 2013), Ligue Régionale contre le Cancer (Midi-Pyrénées), INSERM Transfert, Cancéropôle Grand Sud-Ouest, Rotary Toulouse Clubs, Fondation Toulouse Cancer Santé, and Fondation ARC (Equipe Labellisée 2019). The research leading to these results has received funding from the Transcan-2 Research Program, which is a transnational R&D program jointly funded by national funding organizations within the framework of the ERA-NET Transcan-2 (IMMUSPHINX project). A. Montfort was a recipient of the “Prestige” fellowship program from the Marie Curie Actions (PCOFUNDGA-2013-609102) and is a recipient of a fellowship from Fondation de France.

References

1. Ogretmen B. Sphingolipid metabolism in cancer signalling and therapy. Nat Rev Cancer 2018;18:33–50. [PubMed: 29147025]
2. Hannun YA. The sphingomyelin cycle and the second messenger function of ceramide. J Biol Chem 1994;269:3125–8. [PubMed: 8106344]
3. Milhas D, Clarke CJ, Hannun YA. Sphingomyelin metabolism at the plasma membrane: implications for bioactive sphingolipids. FEBS Lett 2010;584:1887–94. [PubMed: 19857494]
4. Hofmann K, Tomiuk S, Wolff G, Stoffel W. Cloning and characterization of the mammalian brain-specific, Mg2+-dependent neutral sphingomyelinase. Proc Natl Acad Sci U S A 2000;97:5895–900. [PubMed: 10823942]
5. Rutkute K, Karakashian AA, Giltiay NV, Dobierzewska A, Nikolova-Karakashian MN. Aging in rat causes hepatic hyperresposiveness to interleukin-1beta which is mediated by neutral sphingomyelinase-2. Hepatology 2007;46:1166–76. [PubMed: 17668873]
6. Clarke CJ, Truong TG, Hannun YA. Role for neutral sphingomyelinase-2 in tumor necrosis factor alpha-stimulated expression of vascular cell adhesion molecule-1 (VCAM) and intercellular adhesion molecule-1 (ICAM) in lung epithelial cells: p38 MAPK is an upstream regulator of nSMase2. J Biol Chem 2007;282:1384–96. [PubMed: 17085432]
7. Shamseddine AA, Clarke CJ, Carroll B, Airola MV, Mohammed S, Rella A, et al. P53-dependent upregulation of neutral sphingomyelinase-2: role in doxorubicin-induced growth arrest. Cell Death Dis 2015;6:e1947. [PubMed: 26512957]
8. Kim WJ, Okimoto RA, Purton LE, Goodwin M, Haserlat SM, Dayyani F, et al. Mutations in the neutral sphingomyelinase gene SMPD3 implicate the ceramide pathway in human leukemias. Blood 2008;111:4716–22. [PubMed: 18299447]
9. Demircan B, Dyer LM, Gerace M, Lobenhofer EK, Robertson KD, Brown KD. Comparative epigenomics of human and mouse mammary tumors. Genes Chromosomes Cancer 2009;48:83–97. [PubMed: 18836996]
10. Albinet V, Bats ML, Huwiler A, Rochaix P, Chevreau C, Segui B, et al. Dual role of sphingosine kinase-1 in promoting the differentiation of dermal fibroblasts and the dissemination of melanoma cells. Oncogene 2014;33:3364–73. [PubMed: 23893239]
11. Sorli SC, Colie S, Albinet V, Dubrac A, Touriol C, Guilbaud N, et al. The nonlysosomal beta-glucosidase GBA2 promotes endoplasmic reticulum stress and impairs tumorigenicity of human melanoma cells. FASEB J 2013;27:489–98. [PubMed: 23073830]
12. Bedia C, Casas J, Andrieu-Abadie N, Fabrias G, Levade T. Acid ceramidase expression modulates the sensitivity of A375 melanoma cells to dacarbazine. J Biol Chem 2011;286:28200–9. [PubMed: 21700700]
13. Colie S, Van Veldhoven PP, Kedjouar B, Bedia C, Albinet V, Sorli SC, et al. Disruption of sphingosine 1-phosphate lyase confers resistance to chemotherapy and promotes oncogenesis through Bcl-2/Bcl-xL upregulation. Cancer Res 2009;69:9346–53. [PubMed: 19934311]
14. Bilal F, Montfort A, Gilhodes J, Garcia V, Riond J, Carpentier S, et al. Sphingomyelin synthase 1 (SMS1) downregulation is associated with sphingolipid reprogramming and a worse prognosis in melanoma. Front Pharmacol 2019;10:443. [PubMed: 31114500]
15. Imbert C, Montfort A, Fraisse M, Marcheteau E, Gilhodes J, Martin E, et al. Resistance of melanoma to immune checkpoint inhibitors is overcome by targeting the sphingosine kinase-1. Nat Commun 2020;11:437. [PubMed: 31974367]
16. Mrad M, Imbert C, Garcia V, Rambow F, Therville N, Carpentier S, et al. Downregulation of sphingosine kinase-1 induces protective tumor immunity by promoting M1 macrophage response in melanoma. Oncotarget 2016;7:71873–86. [PubMed: 27708249]
17. Garandeau D, Noujarede J, Leclerc J, Imbert C, Garcia V, Bats ML, et al. Targeting the sphingosine 1-phosphate axis exerts potent antitumor activity in BRAFi-resistant melanomas. Mol Cancer Ther 2019;18:289–300. [PubMed: 30482853]
18. Belleri M, Paganini G, Coltrini D, Ronca R, Zizioli D, Corsini M, et al. Beta-galactosylceramidase promotes melanoma growth via modulation of ceramide metabolism. Cancer Res 2020;80:5011–23. [PubMed: 32998995]

19. Larkin J, Chiarion-Sileni V, Gonzalez R, Grob JJ, Cowey CL, Lao CD, et al. Combined nivolumab and ipilimumab or monotherapy in untreated melanoma. N Engl J Med 2015;373:23–34. [PubMed: 26027431]
20. Riker AI, Enkemann SA, Fodstad O, Liu S, Ren S, Morris C, et al. The gene expression profiles of primary and metastatic melanoma yields a transition point of tumor progression and metastasis. BMC Med Genomics 2008;1:13. [PubMed: 18442402]
21. Cancer Genome Atlas Network. Genomic classification of cutaneous melanoma. Cell 2015;161:1681–96. [PubMed: 26091043]
22. Ycart B, Pont F, Fournie JJ. Curbing false discovery rates in interpretation of genome-wide expression profiles. J Biomed Inform 2014;47:58–61. [PubMed: 24060601]
23. Subramanian A, Tamayo P, Mootha VK, Mukherjee S, Ebert BL, Gillette MA, et al. Gene set enrichment analysis: a knowledge-based approach for interpreting genome-wide expression profiles. Proc Natl Acad Sci U S A 2005;102:15545–50. [PubMed: 16199517]
24. Gao J, Aksoy BA, Dogrusoz U, Dresdner G, Gross B, Sumer SO, et al. Integrative analysis of complex cancer genomics and clinical profiles using the cBioPortal. Sci Signal 2013;6:pl1.
25. Cerami E, Gao J, Dogrusoz U, Gross BE, Sumer SO, Aksoy BA, et al. The cBio Cancer Genomics Portal: an open platform for exploring multidimensional cancer genomics data. Cancer Discov 2012;2:401–4. [PubMed: 22588877]
26. Bertrand F, Rochotte J, Colacios C, Montfort A, Tilkin-Mariame AF, Touriol C, et al. Blocking tumor necrosis factor alpha enhances CD8 T-cell-dependent immunity in experimental melanoma. Cancer Res 2015;75:2619–28. [PubMed: 25977337]
27. Porgador A, Feldman M, Eisenbach L. H-2Kb transfection of B16 melanoma cells results in reduced tumourigenicity and metastatic competence. J Immunogenet 1989;16:291–303. [PubMed: 2639904]
28. Meeth K, Wang JX, Micevic G, Damsky W, Bosenberg MW. The YUMM lines: a series of congenic mouse melanoma cell lines with defined genetic alterations. Pigment Cell Melanoma Res 2016;29:590–7. [PubMed: 27287723]
29. Pencheva N, Buss CG, Posada J, Merghoub T, Tavazoie SF. Broad-spectrum therapeutic suppression of metastatic melanoma through nuclear hormone receptor activation. Cell 2014;156:986–1001. [PubMed: 24581497]
30. Tani M, Hannun YA. Analysis of membrane topology of neutral sphingomyelinase 2. FEBS Lett 2007;581:1323–8. [PubMed: 17349629]
31. Subra C, Grand D, Laulagnier K, Stella A, Lambeau G, Paillasse M, et al. Exosomes account for vesicle-mediated transcellular transport of activatable phospholipases and prostaglandins. J Lipid Res 2010;51:2105–20. [PubMed: 20424270]
32. Micheau O, Lens S, Gaide O, Alevizopoulos K, Tschopp J. NF-kappaB signals induce the expression of c-FLIP. Mol Cell Biol 2001;21:5299–305. [PubMed: 11463813]
33. Morgenstern JP, Land H. Advanced mammalian gene transfer: high titre retroviral vectors with multiple drug selection markers and a complementary helper-free packaging cell line. Nucleic Acids Res 1990;18:3587–96. [PubMed: 2194165]
34. Wiegmann K, Schutze S, Machleidt T, Witte D, Kronke M. Functional dichotomy of neutral and acidic sphingomyelinases in tumor necrosis factor signaling. Cell 1994;78:1005–15. [PubMed: 7923351]
35. Bielawski J, Szulc ZM, Hannun YA, Bielawska A. Simultaneous quantitative analysis of bioactive sphingolipids by high-performance liquid chromatography-tandem mass spectrometry. Methods 2006;39:82–91. [PubMed: 16828308]
36. Bertrand F, Montfort A, Marcheteau E, Imbert C, Gilhodes J, Filleron T, et al. TNFalpha blockade overcomes resistance to anti-PD-1 in experimental melanoma. Nat Commun 2017;8:2256. [PubMed: 29273790]
37. Hodis E, Watson IR, Kryukov GV, Arold ST, Imielinski M, Theurillat JP, et al. A landscape of driver mutations in melanoma. Cell 2012;150:251–63. [PubMed: 22817889]
38. Krauthammer M, Kong Y, Ha BH, Evans P, Bacchiocchi A, McCusker JP, et al. Exome sequencing identifies recurrent somatic RAC1 mutations in melanoma. Nat Genet 2012;44:1006–14. [PubMed: 22842228]

39. Shain AH, Garrido M, Botton T, Talevich E, Yeh I, Sanborn JZ, et al. Exome sequencing of desmoplastic melanoma identifies recurrent NFKBIE promoter mutations and diverse activating mutations in the MAPK pathway. Nat Genet 2015;47:1194–9. [PubMed: 26343386]
40. Hoadley KA, Yau C, Hinoue T, Wolf DM, Lazar AJ, Drill E, et al. Cell-of-origin patterns dominate the molecular classification of 10,000 tumors from 33 types of cancer. Cell 2018;173:291–304. [PubMed: 29625048]
41. Airola MV, Shanbhogue P, Shamseddine AA, Guja KE, Senkal CE, Maini R, et al. Structure of human nSMase2 reveals an interdomain allosteric activation mechanism for ceramide generation. Proc Natl Acad Sci U S A 2017;114:E5549–E58. [PubMed: 28652336]
42. Trajkovic K, Hsu C, Chiantia S, Rajendran L, Wenzel D, Wieland F, et al. Ceramide triggers budding of exosome vesicles into multivesicular endosomes. Science 2008;319:1244–7. [PubMed: 18309083]
43. Andre F, Schartz NE, Movassagh M, Flament C, Pautier P, Morice P, et al. Malignant effusions and immunogenic tumour-derived exosomes. Lancet 2002;360:295–305. [PubMed: 12147373]
44. Chen G, Huang AC, Zhang W, Zhang G, Wu M, Xu W, et al. Exosomal PD-L1 contributes to immunosuppression and is associated with anti-PD-1 response. Nature 2018;560:382–6. [PubMed: 30089911]
45. Poggio M, Hu T, Pai CC, Chu B, Belair CD, Chang A, et al. Suppression of exosomal PD-L1 induces systemic anti-tumor immunity and memory. Cell 2019;177:414–27. [PubMed: 30951669]
46. Lim SO, Li CW, Xia W, Cha JH, Chan LC, Wu Y, et al. Deubiquitination and stabilization of PD-L1 by CSN5. Cancer Cell 2016;30:925–39. [PubMed: 27866850]
47. Eppihimer MJ, Gunn J, Freeman GJ, Greenfield EA, Chernova T, Erickson J, et al. Expression and regulation of the PD-L1 immunoinhibitory molecule on microvascular endothelial cells. Microcirculation 2002;9:133–45. [PubMed: 11932780]
48. Hannun YA, Obeid LM. Principles of bioactive lipid signalling: lessons from sphingolipids. Nat Rev Mol Cell Biol 2008;9:139–50. [PubMed: 18216770]
49. Garcia-Barros M, Paris F, Cordon-Cardo C, Lyden D, Rafii S, Haimovitz-Friedman A, et al. Tumor response to radiotherapy regulated by endothelial cell apoptosis. Science 2003;300:1155–9. [PubMed: 12750523]
50. Garcia-Barros M, Lacorazza D, Petrie H, Haimovitz-Friedman A, Cardon-Cardo C, Nimer S, et al. Host acid sphingomyelinase regulates microvascular function not tumor immunity. Cancer Res 2004;64:8285–91. [PubMed: 15548696]
51. Carpinteiro A, Becker KA, Japtok L, Hessler G, Keitsch S, Pozgajova M, et al. Regulation of hematogenous tumor metastasis by acid sphingomyelinase. EMBO Mol Med 2015;7:714–34. [PubMed: 25851537]
52. Bizzozero L, Cazzato D, Cervia D, Assi E, Simbari F, Pagni F, et al. Acid sphingomyelinase determines melanoma progression and metastatic behaviour via the microphtalmia-associated transcription factor signalling pathway. Cell Death Differ 2014;21:507–20. [PubMed: 24317198]
53. Assi E, Cervia D, Bizzozero L, Capobianco A, Pambianco S, Morisi F, et al. Modulation of acid sphingomyelinase in melanoma reprogrammes the tumour immune microenvironment. Mediators Inflamm 2015;2015:370482. [PubMed: 26101462]
54. Matloubian M, Lo CG, Cinamon G, Lesneski MJ, Xu Y, Brinkmann V, et al. Lymphocyte egress from thymus and peripheral lymphoid organs is dependent on S1P receptor 1. Nature 2004;427:355–60. [PubMed: 14737169]
55. Joseph CK, Wright SD, Bornmann WG, Randolph JT, Kumar ER, Bittman R, et al. Bacterial lipopolysaccharide has structural similarity to ceramide and stimulates ceramide-activated protein kinase in myeloid cells. J Biol Chem 1994;269:17606–10. [PubMed: 8021269]
56. Li G, Liu D, Kimchi ET, Kaifi JT, Qi X, Manjunath Y, et al. Nanoliposome C6-ceramide increases the anti-tumor immune response and slows growth of liver tumors in mice. Gastroenterology 2018;154:1024–36. [PubMed: 29408569]
57. Zhang T, de Waard AA, Wuhrer M, Spaapen RM. The role of glycosphingolipids in immune cell functions. Front Immunol 2019;10:90. [PubMed: 30761148]

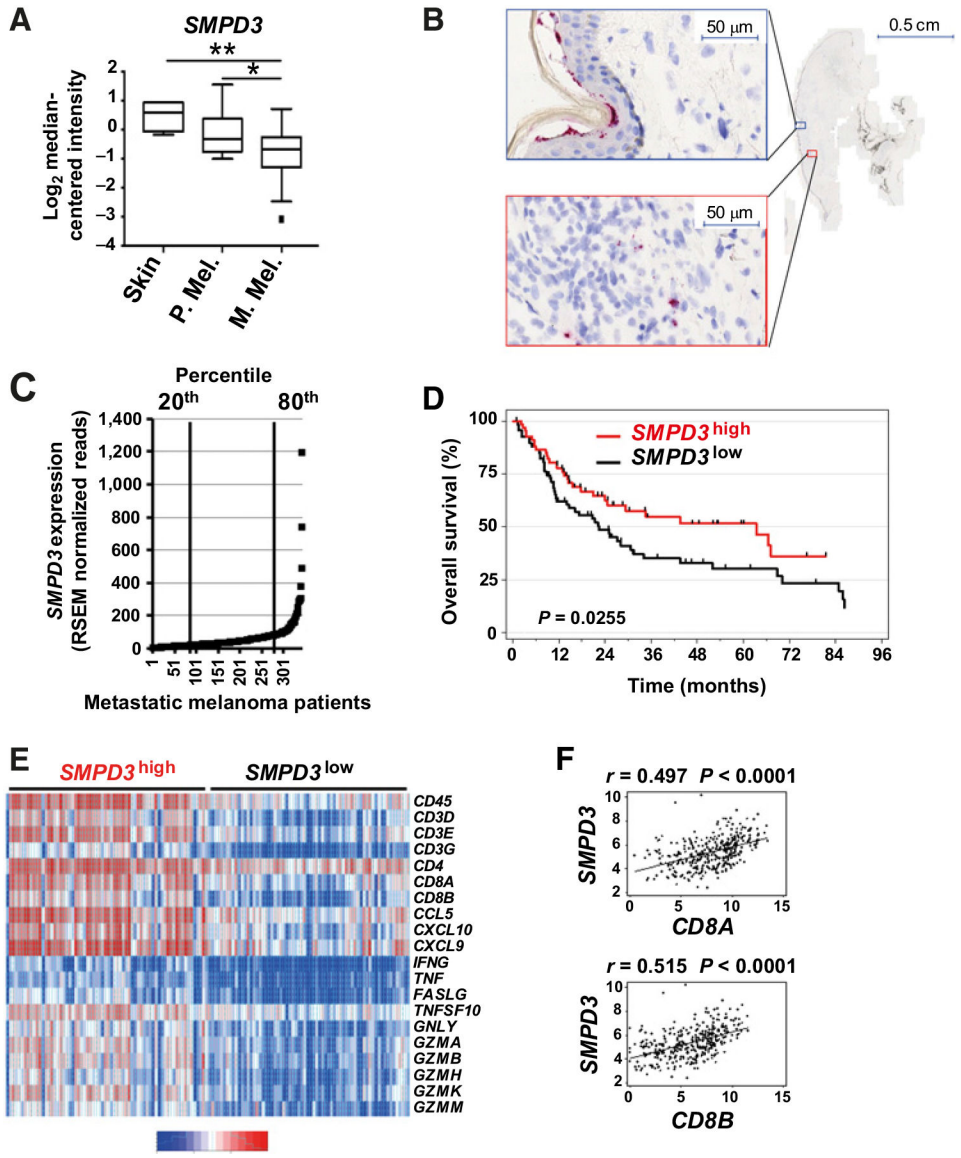

Figure 1.

Low expression of *SMPD3* in patients with melanoma is associated with worse prognosis and low immune gene signatures. **A,** *SMPD3* expression analysis in normal human skin ($n = 4$), primary (P. Mel., $n = 14$), and metastatic (M. Mel., $n = 40$) melanoma samples from the Oncomine database. *, $P < 0.05$; **, $P < 0.01$. **B,** *SMPD3* expression analyzed by ISH on a skin sample from a patient with advanced melanoma. Pictures are representative of staining carried out on samples from five patients. **C,** *SMPD3* expression analysis in tumor biopsies from patients with metastatic melanoma (TCGA melanoma cohort; $n = 342$). RSEM, RNA-Seq by Expectation Maximization. **D,** Overall survival in patients with metastatic melanoma from the TCGA melanoma cohort, exhibiting tumors with high (>80th percentile; $n = 68$) or low (<20th percentile; $n = 68$) *SMPD3* expression in melanoma samples. **E,**, Heatmap depicting the differential expression of a selected set of genes related to immune responses in melanoma biopsies (TCGA) with high (*SMPD3*^{high}) or low

(*SMPD3*^{low}) *SMPD3* expression. Genes were clustered using a Euclidean distant matrix and average linkage clustering. **F,** Correlation analyses of *SMPD3* expression with the indicated genes (TCGA).

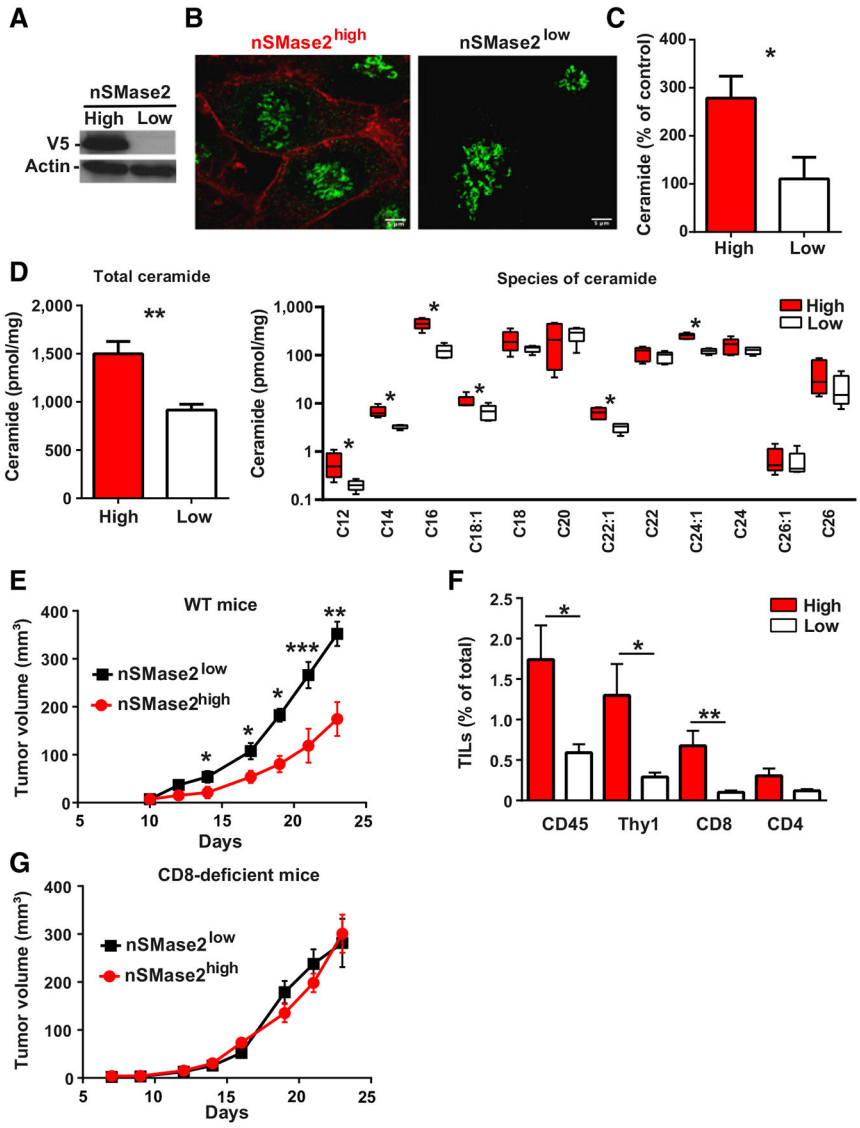

Figure 2.

nSMase2 expression in mouse melanoma enhances CD8$^+$ T-cell–dependent immune responses. **A,** B16K1 cells transfected to overexpress V5-tagged nSMase2 (nSMase2^{high}) or not (nSMase2^{low}) were analyzed by Western blot using anti-V5 and anti–β-actin antibodies. **B,** Confocal microscopy analysis showing V5-tagged nSMase2 (red staining) and giantin (green staining) localization in B16K1 cells expressing nSMase2 at low or high level. **C,** Intracellular ceramide levels in B16K1 nSMase2^{high} and B16K1 nSMase2^{low} cells. Data are expressed as the percentage of values obtained as compared with mock-transfected B16K1 cells. Values are mean ± SEM of four independent experiments. **D–G,** C57BL/6 WT (**D**–**F**) and CD8α-deficient (**G**) mice were intradermally and bilaterally (**D**, **E**, and **G**) or monolaterally (**F**) injected with B16K1 cells expressing high (nSMase2^{high}; red bars, Tukey boxes and curves) or low (nSMase2^{low}; black and white bars, Tukey boxes and curves) levels of nSMase2. **D,** At day 12, WT mice were sacrificed and the levels of total as well as of subspecies of ceramide were analyzed by mass spectrometry (n = 5 tumors/mice per

group, Student *t* test and Kruskal–Wallis). **E,** Tumor volumes in WT mice at the indicated days ($n = 4–5$ mice per group). **F,** Tumor-infiltrating leukocytes were analyzed using flow cytometry at day 12 following tumor graft ($n = 5–6$ mice per group). **G,** Growth of B16K1 nSMase2^{high} and nSMase2^{low} tumor in CD8α-deficient mice. Data are mean ± SEM of five mice per group (*, $P < 0.05$; **, $P < 0.01$; ***, $P < 0.001$).

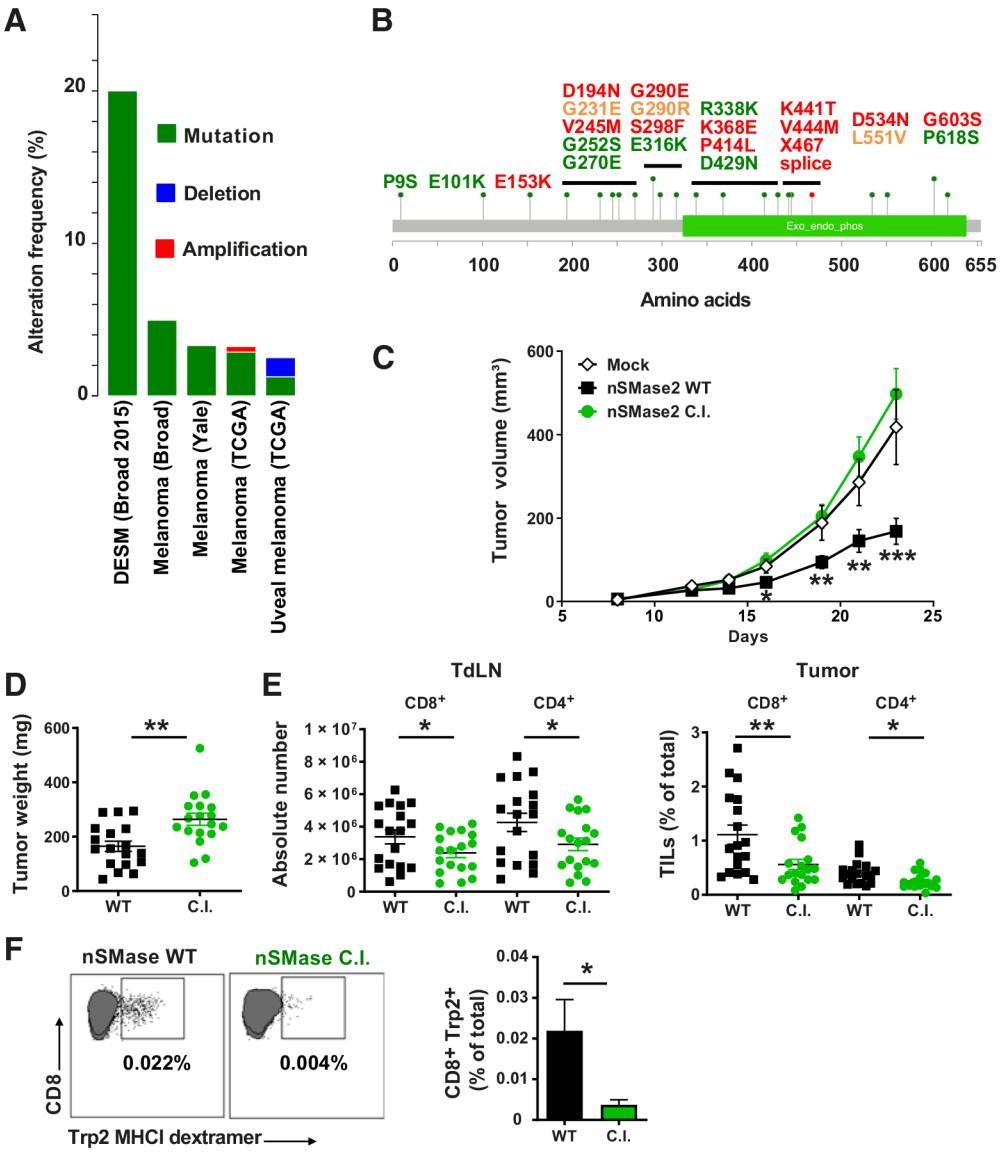

Figure 3.

Catalytic activity is required for nSMase2 to suppress melanoma growth and stimulate immune responses. **A,** Frequency of mutations and copy-number alterations in human melanoma samples from the indicated studies (www.cbioportal.org). **B,** Localization of missense (green dots) and splice (red dot) mutations on nSMase2 amino acid sequence from the studies depicted in **A**. The catalytic site corresponds to the green box. Mutations are predicted to be benign (green), possibly damaging (orange), or probably damaging (red; http://genetics.bwh.harvard.edu/pph2/). **C,** B16K1 cells expressing or not (mock) the WT or C.I. nSMase2 were intradermally injected in C57BL/6 WT mice, and tumor volumes were determined at the indicated days. Data are mean ± SEM of four mice per group (*, $P < 0.05$; **, $P < 0.01$; ***, $P < 0.001$). **D–F,** B16K1 cells expressing the WT or C.I. nSMase2 were intradermally and bilaterally injected in WT mice, and 12 days later, tumor-draining lymph nodes (TdLN) and tumors were collected. Tumors were weighed (**D**), and T-cell content

was analyzed by flow cytometry in TdLNs (**E**, left plot) and tumors (**E**, right plot). Data are mean ± SEM of 18 mice per groups pooled from three independent experiments (**D** and **E**). **F**, $CD8^+$ T cells specific for Trp2 peptides were quantified using dextramer technology. Representative staining and proportion of total Trp2-specific $CD8^+$ T cells are depicted. Numbers are mean ± SEM of six mice per group (*, $P < 0.05$; **, $P < 0.01$).

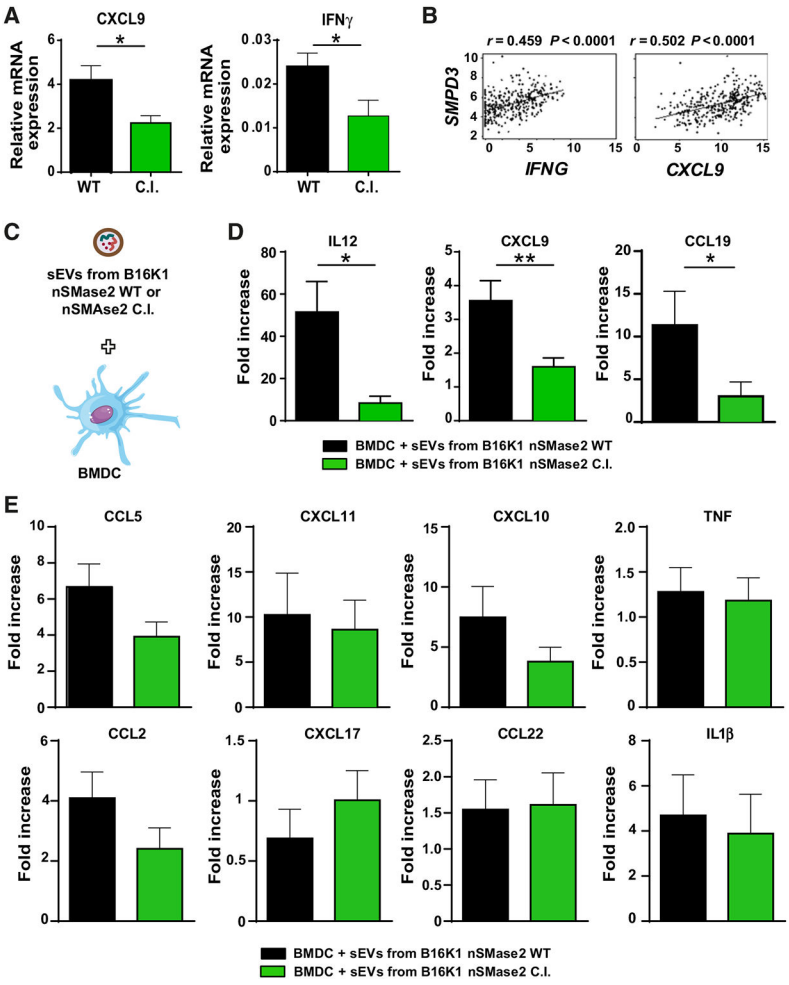

Figure 4.

Melanoma nSMase2 enhances Th1-related gene expression in melanoma tumors and sEV-treated BMDCs. **A,** C57BL/6 mice were injected with B16K1 cells expressing the WT or C.I. form of nSMase2 as described in Fig. 3. At day 12, tumors were harvested, RNAs were purified, and transcripts encoding CXCL9 and IFNγ were analyzed by RT-qPCR. Data are mean ± SEM of eight tumors per group (*, $P < 0.05$). **B,** Correlation analyses of *SMPD3* expression with the expression of genes coding for *IFNG* and *CXCL9* (TCGA melanoma dataset). **C–E,** BMDCs were incubated with or without 5 to 10 μg/mL sEVs (pooled results) from B16K1 expressing either WT or C.I nSMase2 (**C**). After 24 hours, expression of the indicated transcripts by BMDCs was analyzed (**D** and **E**). Data are mean ± SEM of five to nine independent experiments carried out on BMDCs treated with two independent sEV preparations and depicted as the fold increase of expression as compared with untreated control BMDCs (*, $P < 0.05$; **, $P < 0.01$).

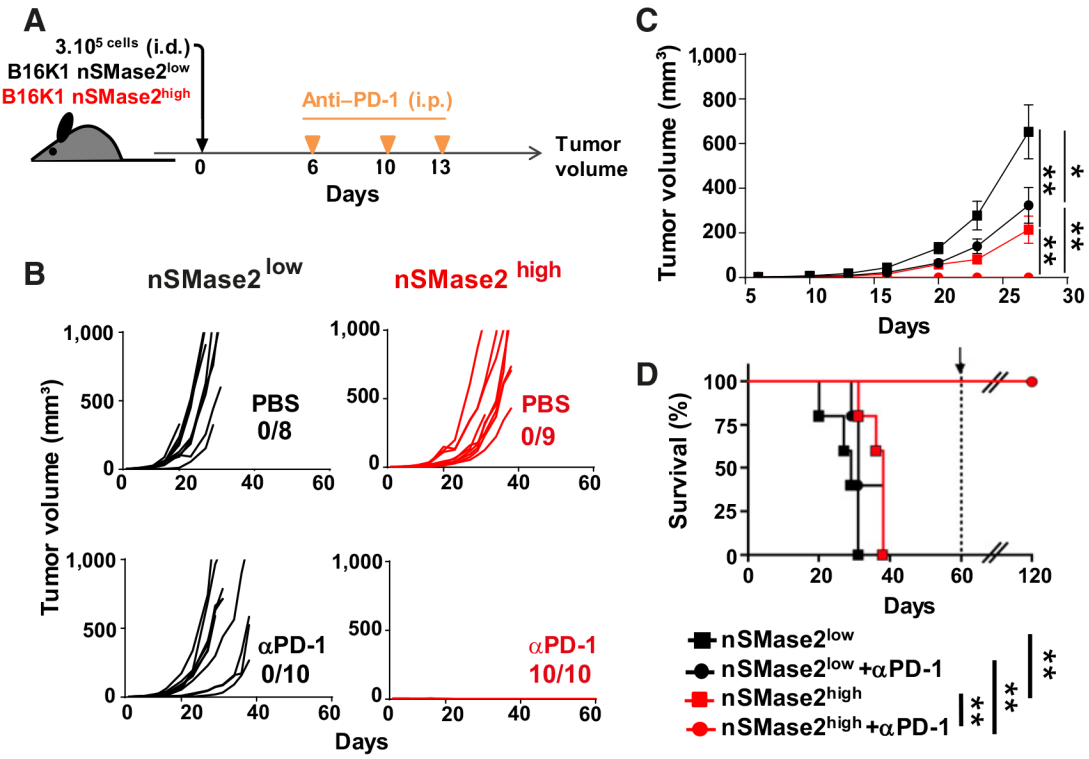

Figure 5.

nSMase 2 potentiates the efficacy of anti–PD-1 therapy *in vivo*. **A–D,** WT mice were intradermally and bilaterally injected with B16K1 expressing high (nSMase2^{high}) or low (nSMase2^{low}) levels of nSMase2 and received i.p. injection of anti–PD-1 (αPD-1; 200 μg) or vehicle (PBS) at days 6, 10, and 13 (5 mice per group, 8–10 tumors; **A**). Individual tumor curves are depicted. Inset, numbers indicate the number of total regressions out of the total number of tumors (**B**). Overall tumor growth analysis in each group. Values are mean ± SEM of 8 to 10 tumors per group (*, $P < 0.05$; **, $P < 0.01$; *t* test; **C**). Overall survival was determined for each group. At day 60, surviving mice were challenged with a second parental B16K1 injection (arrow). Mice did not develop tumors and survived (**D**; *, $P < 0.05$; **, $P < 0.01$; log-rank test).

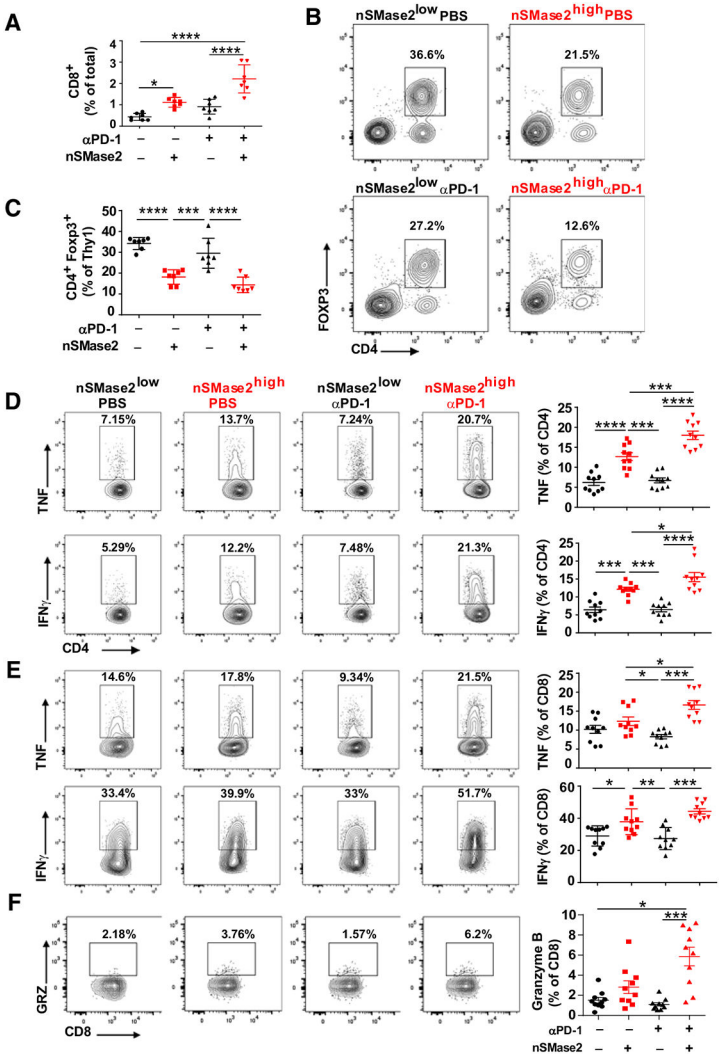

Figure 6.

nSMase2 potentiates the PD-1–dependent immune response in mouse melanoma tumors. **A–D,** nSMase2^{high} or nSMase2^{low} B16K1 cells were bilaterally and intradermally grafted to C57BL/6 WT mice. Mice were then treated with 200 μg of anti–PD-1 or vehicle at day 7 prior to tumor immune infiltrate analysis by flow cytometry at day 10. The two tumors from each mouse were pooled prior to immune cell infiltration analysis. **A–C,** Infiltration of tumors by CD8$^+$ T cells (**A**) and CD4$^+$FoxP3$^+$ regulatory T cells (**B** and **C**; $n = 7$ mice group). **D** and **E**, IFNγ and TNF production by tumor-infiltrating CD4$^+$ (**D**) and CD8$^+$ (**E**) T cells following 4-hour phorbol myristate acetate (PMA)/ionomycin incubation in the presence of a Golgi transport blocker. **F**, Alternatively, proportion of granzyme B$^+$ cells was determined among CD8$^+$ TILs ($n = 10$ mice per group). Statistical analyses: one-way ANOVA; *, $P < 0.05$; **, $P < 0.01$; ***, $P < 0.001$; ****, $P < 0.0001$.

Table 1.

Correlation of *SMPD1–4* expression with immune-related genes.

		IFNG	STAT1	IL12A	IL12B	IRF1	TBX21	CD8A	CD8B	CXCL9
SMPD1	Correlation	−0.032	0.0295	−0.103	−0.021	0.0287	0.0376	−0.001	0.0214	−0.032
	P value	0.553	0.586	0.055	0.689	0.597	0.488	0.975	0.693	0.544
SMPD2	Correlation	0.048	0.019	**−0.231**	0.061	0.067	0.102	0.074	**0.110**	0.012
	P value	0.379	0.728	<0.001	0.259	0.213	0.059	0.172	0.041	0.818
SMPD3	Correlation	**0.459**	**0.312**	**0.125**	**0.499**	**0.502**	**0.538**	**0.497**	**0.515**	**0.502**
	P value	<0.001	<0.001	<0.001	0.0204	<0.001	<0.001	<0.001	<0.001	<0.001
SMPD4	Correlation	**−0.151**	**−0.240**	−0.066	−0.104	**−0.142**	−0.080	**−0.135**	**−0.119**	**−0.211**
	P value	0.005	<0.001	0.218	0.054	0.008	0.135	0.012	0.027	<0.001

Note: The strength of relationship between genes in melanoma samples using Spearman rank correlation coefficient. Significant correlations are highlighted in bold.